

Tuning Long-Lived Mn(II) Upconversion Luminescence through Alkaline-Earth Metal Doping and Energy-Level Tailoring

Xiaowang Liu,* Zhigao Yi, Xian Qin, Hong Liu, Wei Huang,* and Xiaogang Liu*

Crystal-site engineering of hexagonal-phase NaGdF₄:Mn through alkaline-earth metal (A²⁺) doping is used to tune the upconversion luminescence of the Mn²⁺ dopants. Experimental and calculated results show the ability of A²⁺ doping to alter the occupancy site of Mn²⁺ ion from Na⁺ to Gd³⁺, thus enabling an emission change from green (520 nm) to yellow (583 nm) upon excitation at 980 nm. The yellow emission of Mn²⁺ shows a long emission lifetime of 65 ms, more than three times longer than the green emission of Mn²⁺ (20 ms). The combination of tunable long-lived Mn²⁺ emission with lanthanide emission at a single-particle level provides a convenient route to triple transient upconversion color codes upon dynamic excitation, which offers an attractive optical feature particularly suitable for efficient document encoding.

Lanthanide-doped upconversion nanoparticles (UCNPs) with a multiband emission feature upon a single-wavelength excitation have received considerable attention in recent decades because of their potential applications in data storage, bioimaging, cancer therapy, and 3D display.^[1–6] The multiband emission attribute of lanthanides has enabled the ease of multicolor synthesis for UCNPs through control over doping levels or the combination of different types of lanthanide dopants.^[7,8]

Dr. X. W. Liu, Prof. W. Huang
MIIT Key Laboratory of Flexible Electronics (KLoFE) and Xi'an
Institute of Flexible Electronics
Northwestern Polytechnical University
Xi'an 710072, Shaanxi, China
E-mail: iamxwliu@nwpu.edu.cn; iamwhuang@nwpu.edu.cn

Z. Yi, Dr. X. Qin, Prof. X. Liu
Department of Chemistry
National University of Singapore
3 Science Drive 3, Singapore 117543, Singapore
E-mail: chmlx@nus.edu.sg

Prof. H. Liu
Institute for Advanced Interdisciplinary Research (iAIR)
University of Jinan
Jinan 250022, Shandong, China

Prof. W. Huang
Key Laboratory of Flexible Electronics
Institute of Advanced Materials
Jiangsu National Synergetic Innovation Center for Advanced Materials
Nanjing Tech University
Nanjing 211816, China

 The ORCID identification number(s) for the author(s) of this article can be found under <https://doi.org/10.1002/adom.201900519>.

DOI: 10.1002/adom.201900519

However, the multicolor integration relies almost exclusively on the manipulation of relative intensity ratios between the emission peaks. Multicolor tuning of UCNPs through modulating the band position of the emission is highly desirable for their applications in biological detection and imaging. Introducing a different type of emission with a long lifetime into conventional UCNPs is particularly attractive for lifetime-based data encoding. Such nanoparticles could allow the ease of access to a library of transient color codes for multiplexing and data encoding.^[9,10]

Incorporation of Mn²⁺ upconversion luminescence into lanthanide emission at a single-particle level may provide a

much-needed solution for the abovementioned challenge.^[11–13] This is because the radiative transition of ⁴T₁→⁶A₁ of Mn²⁺ is spin-forbidden, allowing the decay lifetime of the optical transition to be much longer than that of lanthanide emitters. Additionally, the emission position and lifetime of Mn²⁺ ions are likely to be modulated by crystal-site engineering. Our primary design is to change the surrounding of the emitting Mn²⁺ ions by doping alkaline-earth metal ions (A²⁺) into the host lattice of hexagonal-phase NaGdF₄ (Figure 1a).^[14] The added dopants can induce variations in the energy gap between the ⁴T₁ and ⁶A₁ energy levels of Mn²⁺ as well as the ionic distance of Mn²⁺ or Gd³⁺, thereby enabling the color tuning of Mn²⁺ emission (Figure 1b). In our design, the promotion of Mn²⁺ ions to excited states could be enabled by trapping the excitation energy from the neighboring excited Gd³⁺ ions that are pumped by an energy migration through a multilayered core-shell nanoparticle (Figure S1, Supporting Information).

To validate our hypothesis, we used Ca²⁺, Mn²⁺-codoped core-shell nanoparticles as a model system. We first prepared a series of NaGdF₄:Ca/Mn (*x*/30 mol%, *x* = 0, 5, 20, 40, and 50) core nanoparticles by a hydrothermal method.^[11] The results showed that a low Ca²⁺ doping concentration (<40 mol%) has a negligible impact on the size and morphology of the core nanoparticles. Transmission electron microscopy (TEM) showed that the main products are short nanorods in these cases (Figure S2a–c, Supporting Information). The diameter and length of the nanorods were estimated to be in the regions of 11–13 and 17–20 nm, respectively. Notably, high-level doping of Ca²⁺ (≈40 mol%) led to a shrinkage in both of the diameter (≈8–9 nm) and length (≈0–12 nm) of the nanorods (Figure S2d, Supporting Information). This morphological change is likely

due to the generation of strong transient electric dipoles on the particle's surface as a result of the heavy substitution of Gd^{3+} with Ca^{2+} . The built up of the electric dipoles, in turn, leads to a slow particle growth rate.^[15,16] X-ray diffraction (XRD) analysis of these products showed a pure hexagonal phase (Figure S3, Supporting Information). A lower-angle shift in the diffraction lines of the products was observed relative to that of Mn^{2+} singly doped ones. We attribute this to Ca^{2+} -induced lattice expansion, indicative of successful Ca^{2+} doping in $\beta\text{-NaGdF}_4\text{:Mn}$ nanoparticles.^[17] A further increase in the doping concentration of Ca^{2+} (50 mol%) yielded hexagonal-phase nanorods as a dominant product, together with a small portion of cubic-phased CaF_2 nanoparticles (Figures S2e and S3, Supporting Information).

The doping levels of Ca^{2+} and Mn^{2+} in the nanoparticles were estimated by inductively coupled plasma atomic emission spectroscopy (ICP-AES). The results showed a big discrepancy between the measured and designed concentrations for both ions. For Ca^{2+} doping, there is a continued increase tendency in the doped nanoparticles upon increasing the concentration in precursor solutions. For Mn^{2+} doping, despite the fixed concentration in the precursor (30 mol%), the measured concentration did not always remain constant across the series. Under a relatively low doping content of Ca^{2+} (20 mol%), the Mn^{2+} concentration was estimated to be ≈ 0.6 mol%, while a higher doping level of Ca^{2+} (40 mol%) led to an obvious increase in the concentration of Mn^{2+} to 1.6 mol% (Table S1, Supporting Information). These results suggest that Mn^{2+} has an intrinsically low solubility in $\beta\text{-NaGdF}_4$, and an improved solubility can be attained upon heavy level doping of Ca^{2+} ions due to the similarity in ionic radius and charge between Mn^{2+} and Ca^{2+} .

We then performed epitaxial growth of double layers of $\text{NaGdF}_4\text{:Yb/Tm}$ (49/1 mol%) and NaYF_4 on these core nanoparticles by a seed-mediated approach (Figure S4, Supporting Information).^[18,19] After the shell growth, monodisperse spherical nanoparticles were produced in all cases with diameters in the range of 20–26 nm. The production of spherical-shaped multilayer nanoparticles is likely due to an oleic acid-assisted etching effect at elevated temperatures (Figure 2a–c and Figure S5, Supporting Information).^[20,21] Note that this effect also led to the disappearance of the cubic-shaped impurities in the $\text{NaGdF}_4\text{:Ca/Mn}$ (50/30 mol%) core nanoparticles (Figure 2d). High-resolution TEM revealed a high crystallinity of the core–shell nanoparticles. A measured d -spacing of the lattice fringes of ≈ 0.27 nm is in accordance with the lattice spacing in the (002) planes of the $\beta\text{-NaGdF}_4$ (Figure S6a, Supporting Information). The core–shell–shell morphology of the as-prepared nanoparticles was further verified by Ca, Yb, and Gd elemental mapping (Figure S6b–d, Supporting Information).

Next, we compared steady emission profiles of the as-prepared multilayer nanoparticles upon excitation at 980 nm (Figure 2e and Figure S7, Supporting Information). Notable

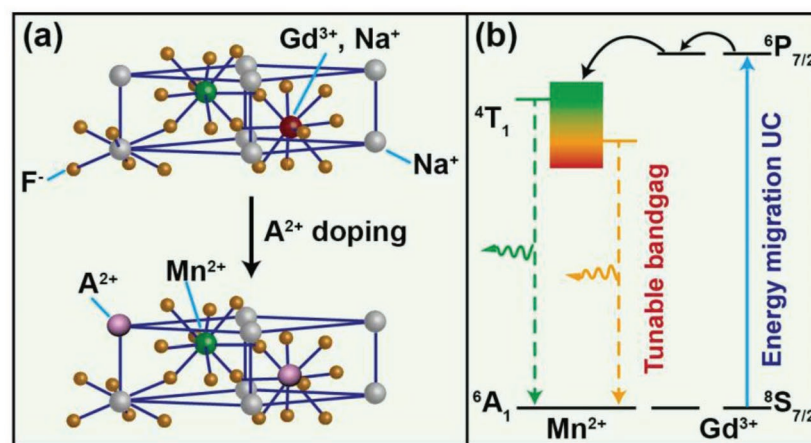


Figure 1. a) Schematic representation of the crystal-site engineering for $\beta\text{-NaGdF}_4\text{:Mn}$ through A^{2+} doping. b) The change in the coordination environment of Mn^{2+} ion enables the variation in the energy level between their ${}^4\text{T}_1$ and ${}^6\text{A}_1$ states and neighboring $\text{Mn}^{2+}\text{-Mn}^{2+}$ distance. This effect, when combined with Gd-sublattice-mediated energy migration, may lead to tunable emission peak position and lifetime of the Mn^{2+} dopant.

changes were observed in the upconverted Mn^{2+} emission. An elevated doping level of Ca^{2+} not only led to a gradual decrease in the overall Mn^{2+} emission intensity but also resulted in a red shift in the emission band (Figure 2f). Specifically, at a 5 mol% doping level of Ca^{2+} , the emission peak appeared at 520 nm. Upon increasing the doping concentration of Ca^{2+} , the emission band gradually broadened (20 mol%) and then split into two different emission peaks (50 mol%) at 520 and 583 nm. We attribute the two emission bands of Mn^{2+} to two different emitting centers upon heavily doping of Ca^{2+} ions, as evident by the observation of two distinct decay kinetics (Figure 2g). The lifetimes for the yellow and green emissions were estimated to be 65 and 20 ms, respectively. The yellow emission displayed a record lifetime for Mn^{2+} as compared with previous reports.^[22,23] Interestingly, the emergence of the new emitting center has a marginal effect on the green emitting sites because it essentially showed unchanged decay kinetics (20 ms) at different doping levels of Ca^{2+} (Figure S8, Supporting Information). Indeed, the changing trend of Mn^{2+} luminescence upon Ca^{2+} doping was further confirmed by luminescence trace recording upon dynamic excitation of the nanoparticles, by which we could observe an obvious transition of the tail emission from green to yellow (Figure 2h). In addition to the changes in the optical properties of Mn^{2+} , the emission intensity of Tm^{3+} is decreased upon enhancing the doping level of Ca^{2+} . We attribute the observation to a slightly increased quenching effect of Mn^{2+} to the luminescence of Tm^{3+} at the interface between the core and the middle layer of the multilayer nanoparticles.^[24]

Based on our results and previous findings, we proposed a luminescence mechanism underlying the $\beta\text{-NaGdF}_4$ upon Ca^{2+} doping (Figure 3a). It was suggested that tetrahedrally (weak crystal field) and octahedrally (strong crystal field) coordinated Mn^{2+} ions tend to give rise to green and orange-to-red emission, respectively.^[25–28] We hypothesized that a continued increase in Ca^{2+} doping concentration might lead to variations in the crystal field around Mn^{2+} ions. To prove this, we performed extended

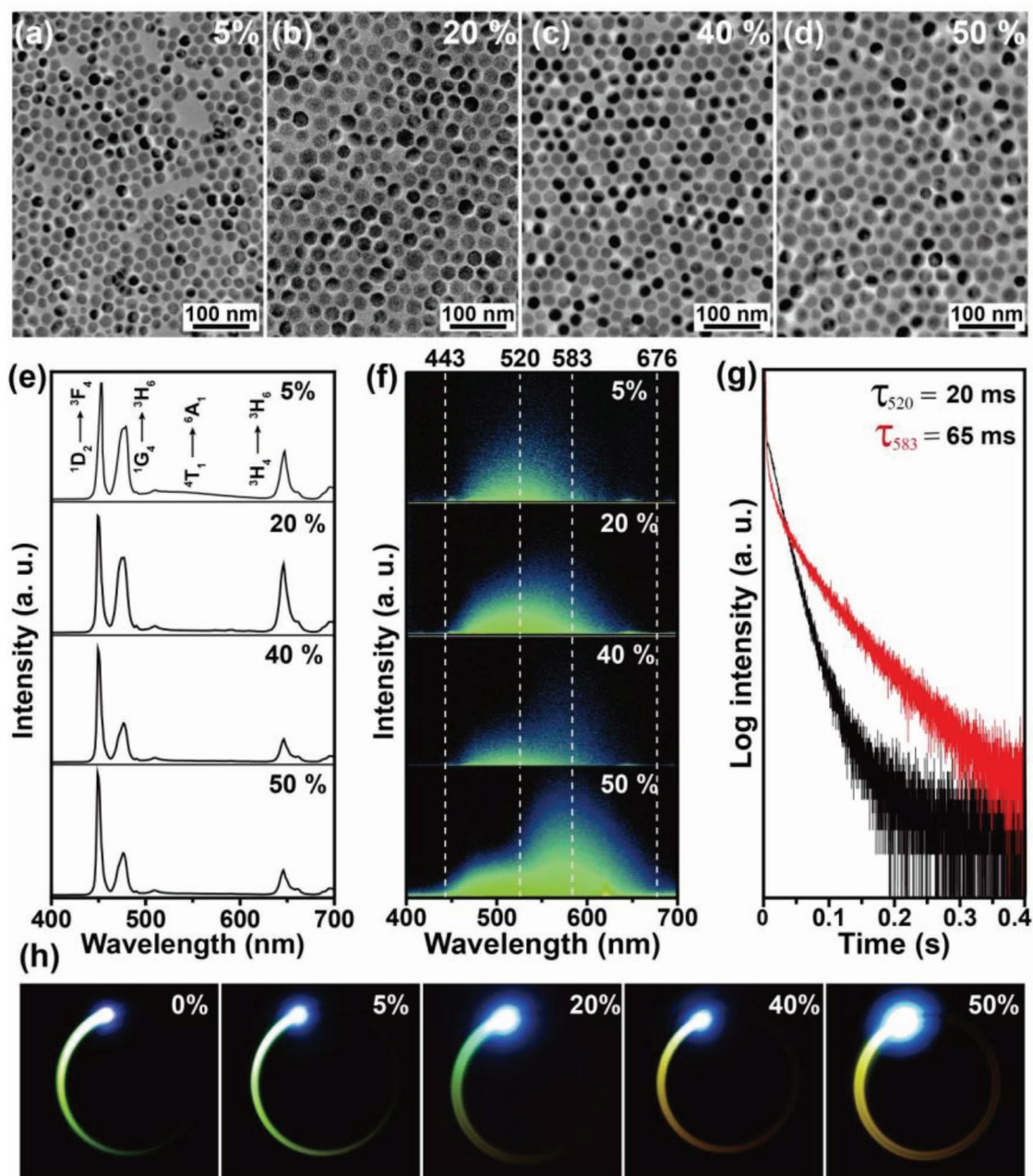


Figure 2. a–d) TEM images of the UCNPs comprising NaGdF₄:Ca/Mn(*x*/30 mol%}@NaGdF₄:Yb/Tm(49/1 mol%}@NaYF₄. e, f) Steady and time-resolved emission spectra of the core–shell–shell nanoparticles under excitation at 980 nm. g) Emission lifetime comparison of Mn²⁺ emissions centered at 520 and 583 nm for NaGdF₄:Ca/Mn(50/30 mol%}@NaGdF₄:Yb/Tm(49/1 mol%}@NaYF₄. The measurement was carried out in an aqueous solution at room temperature. h) Decay luminescence imaging of the nanoparticles upon dynamic excitation at 980 nm (64 W cm⁻²). Note that the samples were spin-coated on cardboard and then mounted onto a rotating motor operating at a spin-speed (ω) of 100 rpm for dynamic excitation.

X-ray absorption fine structure (EXAFS) measurement of NaGdF₄:Ca/Mn (*x*/30 mol%) nanoparticles (*x* = 5 and 40) (Figure 3b). The results (Table S2, Supporting Information) showed that the coordination number of Mn²⁺ increased from 4.1 to 5.9 with an increase in Ca²⁺ doping concentration. The Mn²⁺ ions were found to be surrounded not only by 6 F⁻ ions but also by a Ca²⁺ ion. This arrangement may decrease the Mn²⁺–Mn²⁺ (or Gd³⁺) interaction and allow an ultralong-lived Mn²⁺ emission to be realized at 583 nm.

To provide insight into the crystal site change of Mn²⁺ ions upon Ca²⁺ doping, we evaluated the formation energies of different species, including Ca_Y, Ca_{Na}, Mn_{Na}, and I_F, in β -NaYF₄ through density functional theory (DFT) calculation (Section S2, Supporting information). The use of β -NaYF₄ to replace β -NaGdF₄ in our simulation is because they have virtually the same crystal structure. Also, the approximation can make the calculation much easier due to the less quantity of Y valence electrons, especially considering the formation of various defect

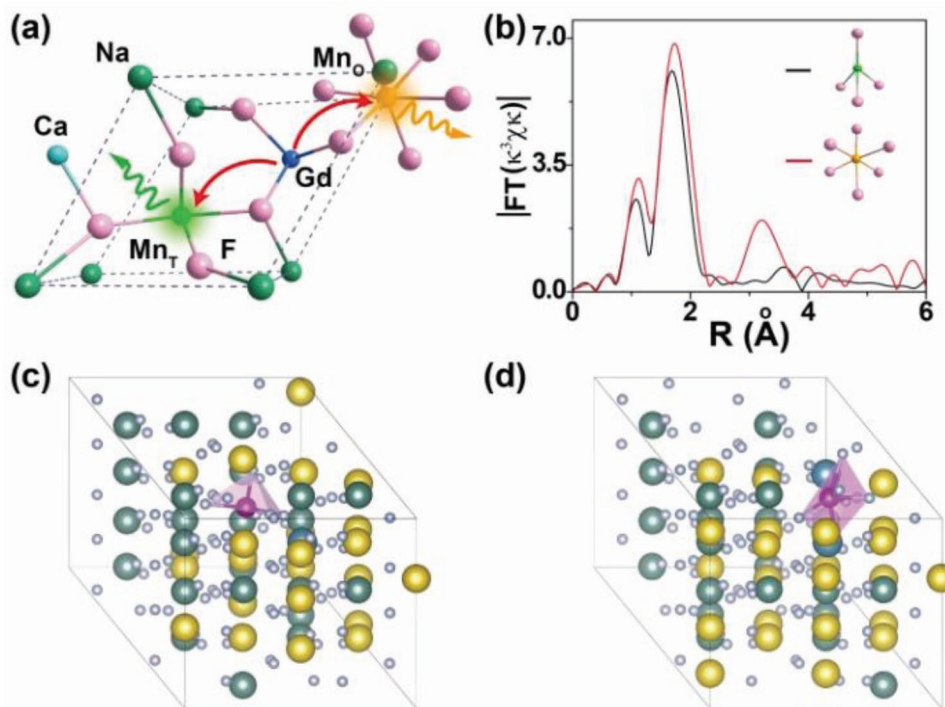


Figure 3. a) Proposed luminescing mechanism of Mn²⁺ in β -NaGdF₄ upon Ca²⁺ doping. High-level Ca²⁺ doping leads to an increase in the coordination number of Mn²⁺ from 4 to 6, with a color change from green to yellow. b) EXAFS of Mn²⁺ in NaGdF₄:Ca/Mn ($x/30$ mol%) NPs ($x = 5$, black line and $x = 40$, red line). c, d) The optimized crystal structures of β -NaYF₄:Mn at low and high Ca²⁺ doping levels from DFT calculation. The calculated results provide substitution tendency of Mn²⁺ in β -NaGdF₄ upon Ca²⁺ doping. Note that Na⁺, Y³⁺, Mn²⁺, and F⁻ are in yellow, cyan, rosy, and grey, respectively.

complexes in the supercells. Importantly, We found that Ca²⁺ and Mn²⁺ dopants have the same substitution behavior in both β -NaYF₄ and β -NaGdF₄ upon separated doping. At a low doping level of Ca²⁺, Ca²⁺, and Mn²⁺ ions prefer to substitute Y³⁺ and Na⁺ sites, leading to the formation of Ca_Y and Mn_{Na} complexes (Table S3, Supporting Information). Under such conditions, the coordination number is optimized to be ≈ 4 by minimizing the formation energy of the doubly doped system (Figure 3c). In contrast, heavy doping of Ca²⁺ ions leads to a significant substitution of Na⁺ ions with Ca²⁺ (Ca_{Na}), alongside a preferential replacement of Y³⁺ sites by Mn²⁺ (Y_{Mn}). The charge neutrality is maintained by the formation of F⁻ vacancies during the substitution in the cell lattice. As such, the coordination number of Mn²⁺ is then increased to ≈ 6 (Figure 3d). Taken together, these experimental and calculation results support the applicability of tuning UC luminescence of Mn²⁺ in β -NaGdF₄ by Ca²⁺ doping at the single-particle level.

To test the robustness of our strategy, other alkaline-earth metals, such as Mg²⁺, Sr²⁺, and Ba²⁺, were used to replace Ca²⁺ in the multilayered NPs. The results showed that Mg²⁺ dopants have the same ability to tune the color output of Mn²⁺ ions from green to yellow (Figures S9–S11, Supporting Information). However, other attempts were unsuccessful mostly because of the poor stability of the core nanoparticles in the presence of a massive doping level of Sr²⁺ or Ba²⁺ (40 mol%), imposing a synthetic challenge for growing multishells (Figures S12–S14, Supporting Information).

The integration of tunable long-lived Mn²⁺ UC emission and other lanthanide emissions at a single-particle level enables the

ease of creating multiple transient color elements for efficient data storage. As a proof-of-concept demonstration, we compared the performance of our Mn²⁺-doped and conventional UCNPs in data encoding (Figures S15 and S16, Supporting Information). A set of 2D covert patterns were fabricated on a card by making use of these nanoparticles as ink solutions (Figure 4a). Upon steady irradiation (Figure 4b), the patterns showed a characteristic color output of lanthanides (patterns i and ii) or a mixed color of lanthanides and Mn²⁺ (patterns iii and iv). Notably, the patterns ii, iii, and iv displayed a similar whitish color readout as a result of a strong emission of Tm³⁺ from the nanoparticles. In contrast, dynamic excitation yielded marked differences in the optical readout (Figure 4c).^[29] We only observed a main spot emission from pattern i made of NaYF₄:Yb/Er nanoparticles. Meanwhile, we observed a binary timescale color codes from pattern ii (a bright spot and a tailed emission) which were made of NaGdF₄:Yb/Tm (49/1 mol%)@NaGdF₄:Eu (15 mol%) nanoparticles. Multicolored luminescence trajectories were observed from patterns iii and iv. The luminescence trajectories can be essentially considered as triple transient color codes based on the change in color output from white to orange to yellow at different time intervals. The generation of such an optical scenario is a result of gradual disappearance the emissions of Tm³⁺, Eu³⁺, and Mn²⁺ along the luminescence traces. This argument was manifested by emission spectroscopy of points 1, 2, and 3 (Figure 4d). These results highlight the flexibility in the creation of multiple transient color elements by making use of tunable Mn²⁺ luminescence.

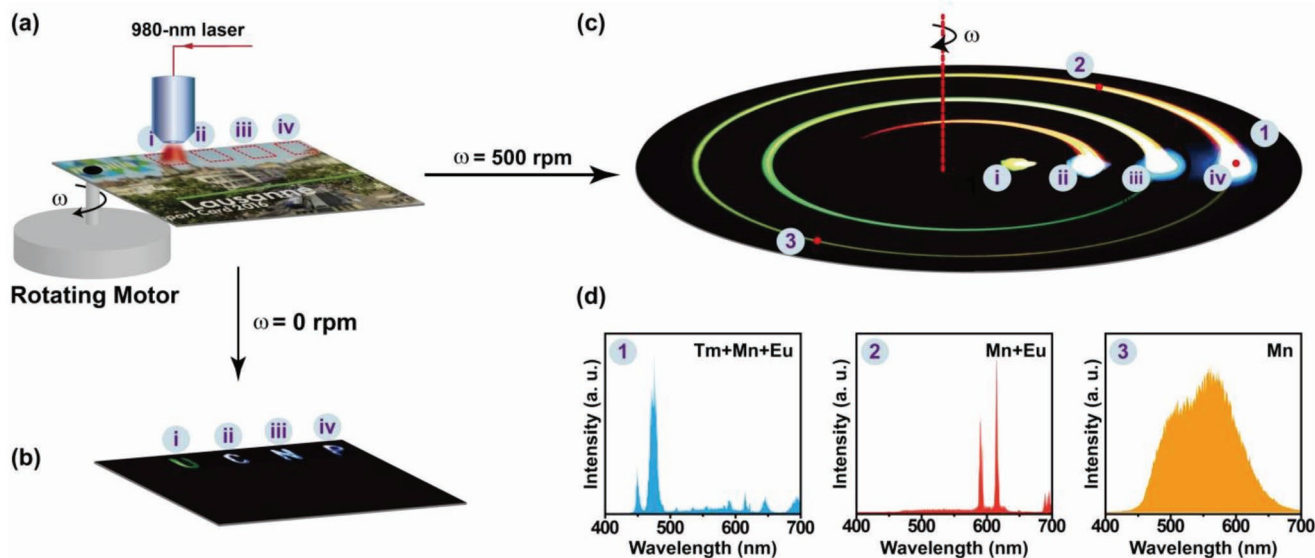


Figure 4. a) Demonstration of Ca^{2+} , Mn^{2+} -codoped multilayer nanoparticles for multilevel data encryption. a) Schematic representation of the creation of 2D covert patterns on a card using different types of UCNPs. Note that the card was fixed on a spin-speed controllable rotor prior to performing dynamic excitation. i) $\text{NaYF}_4:\text{Yb}/\text{Er}$ (20/2 mol%), ii) $\text{NaGdF}_4:\text{Yb}/\text{Tm}$ (49/1 mol%)@ $\text{NaGdF}_4:\text{Eu}$ (15 mol%), iii,iv) $\text{NaGdF}_4:\text{Ca}/\text{Mn}$ ($x/30$ mol%)@ $\text{NaGdF}_4:\text{Yb}/\text{Tm}$ (49/1 mol%)@ $\text{NaYF}_4:\text{Eu}$ (15 mol%), iii, $x = 0$, and iv, $x = 50$. b,c) Optical scenarios of the patterns generated upon steady ($\omega = 0$ rpm, 6 W cm^{-2}) and dynamic ($\omega = 500$ rpm, 64 W cm^{-2}) excitation. d) Emission profiles measured at different points (1, 2, and 3) along the luminescence trajectory iv, as indicated in c.

In conclusion, we have developed a versatile method for tuning the luminescence properties of Mn^{2+} in multilayer nanoparticles through Ca^{2+} or Mg^{2+} doping. Elevation of the doping levels of these metal ions can lead to an increase in the crystal field around Mn^{2+} ions and thus enables the change in the color output from green to yellow, accompanied by an increase in the luminescence lifetime. The emergence of tunable long-lived, upconverted Mn^{2+} emission provides an added temporal code to broaden the application of conventional lanthanide-doped UCNPs in data storage, bioimaging, and multiplexing.

Experimental Section

Experimental details and characterization of as-prepared core and multilayer nanoparticles are available in the Supporting Information.

Supporting Information

Supporting Information is available from the Wiley Online Library or from the author.

Acknowledgements

This study was supported by the Fundamental Research Funds for the Central Universities, the Singapore Ministry of Education (R-143-000-A31-112) and A*STAR (R-143-000-A34-305). The authors thank Dr. Soujie Liu at Anhui Normal University for the EXAFS measurement.

Conflict of Interest

The authors declare no conflict of interest.

Keywords

anti-counterfeiting, codoped nanoparticles, long-lived luminescence, multilayer nanoparticles, transition metals, upconversion

Received: March 26, 2019

Revised: April 7, 2019

Published online:

- [1] F. Auzel, *Chem. Rev.* **2004**, *104*, 139.
- [2] G. Chen, H. Qiu, P. N. Prasad, X. Chen, *Chem. Rev.* **2014**, *114*, 5161.
- [3] H. Dong, S. Du, X. Zheng, G. Lyu, L. Sun, L. Li, P. Zhang, C. Zhang, C. Yan, *Chem. Rev.* **2015**, *115*, 10725.
- [4] W. Zheng, P. Huang, D. Tu, E. Ma, H. Zhu, X. Chen, *Chem. Soc. Rev.* **2015**, *44*, 1379.
- [5] M. Tsang, G. Bai, J. Hao, *Chem. Soc. Rev.* **2015**, *44*, 1585.
- [6] M. Haase, H. Schäfer, *Angew. Chem., Int. Ed.* **2011**, *50*, 5808.
- [7] X. Li, F. Zhang, D. Zhao, *Chem. Soc. Rev.* **2015**, *44*, 1346.
- [8] X. Chen, D. Peng, Q. Ju, F. Wang, *Chem. Soc. Rev.* **2015**, *44*, 1318.
- [9] Y. Lu, J. Zhao, R. Zhang, Y. Liu, D. Liu, E. M. Goldys, X. Yang, P. Xi, A. Sunna, J. Lu, Y. Shi, R. C. Leif, Y. Huo, J. Shen, J. A. Piper, J. P. Robinson, D. Jin, *Nat. Photonics* **2014**, *8*, 32.
- [10] Y. Lu, J. Lu, J. Zhao, J. Cusido, F. M. Raymo, J. Yuan, S. Yang, R. C. Leif, Y. Huo, J. A. Piper, J. P. Robinson, E. M. Goldys, D. Jin, *Nat. Commun.* **2014**, *5*, 3741.
- [11] X. Liu, Y. Wang, X. Li, Z. Yi, R. Deng, L. Liang, X. Xie, D. T. B. Loong, S. Song, D. Fan, A. H. All, H. Zhang, L. Huang, X. Liu, *Nat. Commun.* **2017**, *8*, 899.
- [12] X. Li, X. Liu, D. M. Chevrier, X. Qin, X. Xie, S. Song, H. Zhang, P. Zhang, X. Liu, *Angew. Chem., Int. Ed.* **2015**, *54*, 13312.
- [13] T. Hu, H. Lin, J. Xu, B. Wang, J. Wang, Y. Wang, *J. Mater. Chem. C* **2017**, *5*, 1479.
- [14] E. Song, Z. Chen, M. Wu, S. Ding, S. Ye, S. Zhou, Q. Zhang, *Adv. Opt. Mater.* **2016**, *4*, 798.

- [15] D. Chen, Y. Yu, F. Huang, P. Huang, A. Yang, Y. Wang, *J. Am. Chem. Soc.* **2010**, *132*, 9976.
- [16] L. Lei, D. Chen, P. Huang, J. Xu, R. Zhang, Y. Wang, *Nanoscale* **2013**, *5*, 11298.
- [17] S. Zeng, Z. Yi, W. Lu, C. Qian, H. Wang, L. Rao, T. Zeng, H. Liu, H. Liu, B. Fei, J. Hao, *Adv. Funct. Mater.* **2014**, *24*, 4051.
- [18] X. Li, D. Shen, J. Yang, C. Yao, R. Che, F. Zhang, D. Zhao, *Chem. Mater.* **2013**, *25*, 106.
- [19] N. J. J. Johnson, A. Korinek, C. Dong, F. C. J. M. van Veggel, *J. Am. Chem. Soc.* **2012**, *134*, 11068.
- [20] C. Zhang, J. Y. Lee, *ACS Nano* **2013**, *7*, 4393.
- [21] X. Liu, X. Li, X. Qin, X. Xie, L. Huang, X. Liu, *Adv. Mater.* **2017**, *29*, 1702315.
- [22] E. Song, S. Ding, M. Wu, S. Ye, F. Xiao, S. Zhou, Q. Zhang, *Adv. Opt. Mater.* **2014**, *2*, 670.
- [23] E. Song, S. Ye, T. Liu, P. Du, R. Si, X. Jing, S. Ding, M. Peng, Q. Zhang, L. Wondraczek, *Adv. Sci.* **2015**, *2*, 1500089.
- [24] J. Wang, F. Wang, C. Wang, Z. Liu, X. Liu, *Angew. Chem., Int. Ed.* **2011**, *50*, 10369.
- [25] Y. Y. Ma, J. Q. Hu, E. H. Song, S. Ye, Q. Y. Zhang, *J. Mater. Chem. C* **2015**, *3*, 12443.
- [26] R. Martín-Rodríguez, R. Valiente, M. Bettinelli, *Appl. Phys. Lett.* **2009**, *95*, 091913.
- [27] H. Lin, R. Zhang, D. Chen, Y. Yu, A. Yang, Y. Wang, *J. Mater. Chem. C* **2013**, *1*, 1804.
- [28] E. H. Song, J. L. Wang, D. C. Yu, S. Ye, Q. Y. Zhang, *J. Mater. Chem. C* **2014**, *2*, 8811.
- [29] H. Dong, L. Sun, W. Feng, Y. Gu, F. Li, C. Yan, *ACS Nano* **2017**, *11*, 3289.